JOURNAL OF COMPUTATIONAL PHYSICS 120, 316–322 (1995)

Nonlinear Leapfrog Instability for Fornberg's Pattern

AKIRA AOYAGI

Kyushu Sangyo University, Faculty of Engineering, 3-1 Matsukadai 2-chome, Higashi-ku, Fukuoka 813, Japan

Received September 2, 1994; revised February 17, 1995

The instability of Fornberg's pattern for leapfrog time integration of the nonlinear convective equation $\partial u/\partial t + u\partial u/\partial x = 0$ is found to occur as a closed three-mode process and to include the side-band instability. The perturbation about Fornberg's pattern is able to be unstable for both physical and computational modes. The growth rates as well as the excitation mode spectra of the perturbation are shown to agree with experimental results. © 1995 Academic Press, Inc.

1. INTRODUCTION

The leapfrog scheme used extensively for time integration of partial differential equations has both advantages and drawbacks. Its main advantage is that the scheme is free from dissipation errors. This nondissipative nature of the leapfrog scheme, however, entails the unfavorable feature that it often suffers from numerical instabilities. For a long-time integration of nondissipative equations such as the Korteweg–de Vries equation, it is of practical importance to suppress the instabilities without causing damage to the nondissipative nature. Although the numerical instabilities arising in the leapfrog scheme have been studied from several viewpoints [1–7], few cases are known where the growth mechanisms are clarified by cleanly separating the physical and computational modes of the leapfrog solutions. A better understanding of the mechanism of the instabilities is important when we control the instabilities and get an insight for developing new schemes which are both nondissipative and stable.

In the previous papers, we showed that the leapfrog instability came from the computational mode instability for time integration of the Korteweg–de Vries equation [8, 9] and the van der Pol equation [10]. The computational mode was parametrically excited through nonlinear interactions with the physical mode. It should be noted that the leapfrog solutions in the nonlinear case are also given by the sum of the physical and computational modes as in the linear case. The computational mode has a distinct character of changing sign at each time step. By making use of this character, we can numerically extract the physical and computational modes from the solutions. The unstable leapfrog solutions, which are due to the computational mode instability, can be readily suppressed by eliminating the computational mode from the solutions [9, 10].

In this paper we consider the unstable behavior of Fornberg's pattern for leapfrog time integration of the nonlinear convective equation [1]. We limit our discussion only to the case of $\theta = \frac{2}{3}$ (the parameter θ was introduced by Fornberg and will be explained later). The leapfrog instability arising in this particular case has been treated by Briggs *et al.* [4] and briefly by Sanz-Serna [7]. Briggs *et al.* analyzed the exact leapfrog solutions composed of one, two, three, and four Fourier high-harmonic modes which are able to become nonlinearly unstable. Sanz-Serna discussed the unstable behavior of the two-mode solutions based on the so-called augmented system. According to Briggs *et al.* and also to Fornberg, $\theta = \frac{2}{3}$ is a stability condition for the one-mode solution (i.e., Fornberg's pattern). However, the numerical experiments show that this condition is not enough to suppress the unstable behavior of Fornberg's pattern. For perturbational treatment of the leapfrog instability, it is of key importance to take into account the computational mode as well as the physical mode. We show that a small perturbation about Fornberg's pattern becomes unstable for both physical and computational modes through nonlinear interactions with the stationary fundamental mode and the perturbation itself. This instability basically occurs as the closed three-mode process discussed by Briggs *et al.* [4], and includes the side-band instability introduced by Sloan *et al.* [5]. Since, in our case, one of the three modes is stationary, the problem mainly becomes a linear one. This enables us to calculate the growth rate of the unstable mode dependent upon its mode number. The theoretical growth rates for both physical and computational modes of the perturbation, as well as their excitation spectra, are shown to agree well with experimental results.

The outline of this paper is as follows. In Section 2 we make a numerical demonstration of the leapfrog instability for Fornberg's pattern. The leapfrog solutions are traced separately for the physical and computational modes. To explain the numerical results, in Section 3 we derive the evolution equations for the physical and computational modes of the perturbation about Fornberg's pattern. Section 4 is devoted to an analysis of the unstable solutions for the perturbation. Finally, conclusions are given in Section 5.

0021-9991/95 $12.00

2. NUMERICAL RESULTS OF THE INSTABILITY

We consider 1-periodic in space solutions of nonlinear convective equation,

$$\frac{\partial u}{\partial t} + u\frac{\partial u}{\partial x} = 0 \quad (0 \le x \le 1). \tag{1}$$

Equation (1) can be rewritten as

$$\frac{\partial u}{\partial t} + \frac{\theta}{2}\frac{\partial u^2}{\partial x} + (1-\theta)\,u\frac{\partial u}{\partial x} = 0, \tag{2}$$

using the parameter θ of an arbitrary value [1]. The leapfrog discretization of Eq. (2) gives

$$u_j^{n+1} = u_j^{n-1} - \frac{\Delta t}{2\Delta x}[\theta u_{j+1}^n + 2(1-\theta)u_j^n + \theta u_{j-1}^n](u_{j+1}^n - u_{j-1}^n), \tag{3}$$

where Δt is the time increment, n is the time step, Δx is the grid spacing, and j is the grid number.

Equation (3) has a closed one-mode solution [4] of the form

$$u_j^n = a(n)e^{i(2\pi/3)j} + a^*(n)e^{-i(2\pi/3)j}, \tag{4}$$

where $i = \sqrt{-1}$ and the asterisk denotes complex conjugate, and $a(n)$ is given by the difference relation

$$a(n+1) = a(n-1) + i\frac{\sqrt{3}\Delta t}{2\Delta x}(2-3\theta)a^*(n)^2.$$

We thus have a particular solution for u_j^n in Eq. (3) which is nonlinearly unstable when $\theta \neq \frac{2}{3}$.

To avoid this particular instability we usually take $\theta = \frac{2}{3}$, which also assures the conservation relation

$$\sum_j u_j^{n+1} u_j^n = \text{const.} \tag{5}$$

When $\theta = \frac{2}{3}$, Eq. (3) becomes

$$u_j^{n+1} = u_j^{n-1} - \frac{\Delta t}{3\Delta x}(u_{j+1}^n + u_j^n + u_{j-1}^n)(u_{j+1}^n - u_{j-1}^n). \tag{6}$$

It is obvious from the above discussion that Eq. (6) has a stationary solution for u_j^n in Eq. (4),

$$a(n+1) = a(n-1) = a = \text{const.}$$

If we set $a = i\varepsilon/\sqrt{3}$, the stationary solution is reduced to

$$u_j^n = -\frac{2\varepsilon}{\sqrt{3}}\sin\left(\frac{2\pi}{3}j\right). \tag{7}$$

The constant ε represents the amplitude of u_j^n. The sequence u_j^n for $j = 0, 1, 2, \ldots$, gives the following Fornberg's pattern [1]:

$$\{u_j^n\} = 0, -\varepsilon, \varepsilon, 0, -\varepsilon, \varepsilon, 0, \ldots .$$

If we take Fornberg's pattern as the initial values of Eq. (6), we expect that Eq. (6) wil generate a stationary solution whose pattern remains unchanged in the course of time.

We made numerical integrations based on Eq. (6) with periodic boundary conditions, starting with Fornberg's pattern as the initial values. To control the initial background noise, we added a uniform random noise $\{r_j\}$ of order 10^{-11} to Fornberg's pattern. The computations were made with double precision (15 significant digits), fixing the parameters as $\Delta x = 1/(2J)$, $2J = 120$, and $\Delta t = 0.002$ ($\Delta t/\Delta x = 0.24$), where $2J$ is the total number of grid points. The missing starting values were calculated using the Runge–Kutta scheme. Figure 1a shows that Fornberg's pattern which is marked with round dots remains unchanged up to about the time step $n = 3200$ for $\varepsilon = 0.1$. When the time step exceeds about $n = 3200$, however, the initial pattern begins to suffer a gradual change due to the leapfrog instability as shown in Fig. 1b. If we continue the computation, it blows up at about $n = 3700$ ($t \simeq 7.4$). Figure 2 shows the temporal change of the invariant of Eq. (1),

$$C_2 = \int_0^1 u^2(x,t)\,dx \simeq \Delta x \sum_j u_j^{n2}. \tag{8}$$

The invariant C_2 exhibits an exponential growth for the time steps exceeding about $n = 3400$ ($t \simeq 6.8$). The conservation relation of Eq. (5) holds with remarkable accuracy during the computation.

Now let us decompose the leapfrog solution u_j^n of Eq. (6) into the physical and computational modes,

$$u_j^n = -\frac{2\varepsilon}{\sqrt{3}}\sin\left(\frac{2\pi}{3}j\right) + v_j^n + (-1)^n w_j^n. \tag{9}$$

The perturbations of the physical mode v_j^n and the computational mode w_j^n about Fornberg's pattern can be experimentally obtained from the leapfrog solutions u_j^n and u_j^{n-1} by the aid of the Runge–Kutta integration of the differential version of Eq. (6) [8–10],

$$\frac{du_j}{dt} = -\frac{1}{6\Delta x}(u_{j+1} + u_j + u_{j-1})(u_{j+1} - u_{j-1}).$$

We integrate the above differential equation in the interval of one time step Δt by the Runge–Kutta scheme taking u_j^{n-1} as

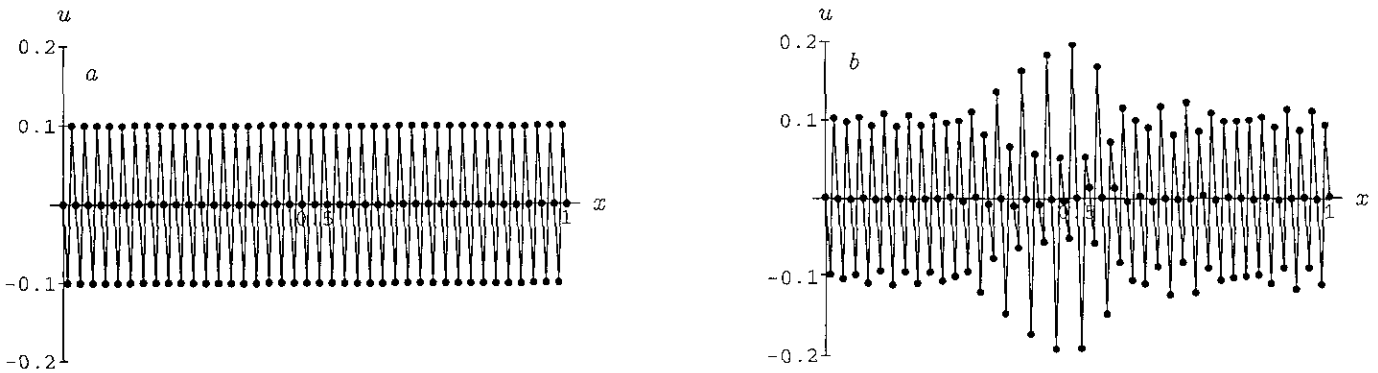

FIG. 1. Numerical solutions of u at (a) $n = 3200$; (b) $n = 3460$ based on Eq. (17) starting with Fornberg's pattern. $\Delta x = \frac{1}{120}$, $\Delta t = 0.002$ ($\Delta t/\Delta x = 0.24$), and $\varepsilon = 0.1$.

the initial values at $t = (n-1)\Delta t$ to obtain u_j ($t = n\Delta t$). Then v_j^n and w_j^n are obtained from the relations

$$v_j^n = \frac{1}{2}[u_j^n + u_j(t = n\Delta t)] + \frac{2\varepsilon}{\sqrt{3}} \sin\left(\frac{2\pi}{3} j\right),$$

$$w_j^n = (-1)^n \frac{1}{2}[u_j^n - u_j(t = n\Delta t)].$$

We thus obtain C_{2p} and C_{2c} defined by

$$C_{2p} \equiv \sqrt{\Delta x \sum_j v_j^{n2}}, \quad C_{2c} \equiv \sqrt{\Delta x \sum_j w_j^{n2}},$$

corresponding to C_2 in Fig. 2. The resulting C_{2p} and C_{2c} are shown as functions of time in Fig. 3. It is seen that C_{2c} grows exponentially with the almost constant growth rate $\gamma \simeq 3.9$, until it blows up. By contrast, C_{2p} first exhibits an oscillatory exponential growth with the growth rate 1.9, and after the time step about 3000 ($t \simeq 6$) it quickly grows with the growth rate 8.1 without oscillation. These values of growth rates are nearly equal to those of $\gamma/2 \simeq 1.95$ and $2\gamma \simeq 7.8$, respectively. The period of oscillation is found to be 1.8 (900 time steps).

It is interesting to note that if we change the value of ε from positive ($\varepsilon = 0.1$) to negative ($\varepsilon = -0.1$), the behavior of C_{2p} and C_{2c} is interchanged as shown in Fig. 4. In this case C_{2p} exhibits the exponential growth with the almost constant growth rate ($\simeq\gamma$), while C_{2c} exhibits the oscillatory change with the growth rate about $\gamma/2$. The quick growth in the final stage of C_{2p} is not observed in this case, and on the contrary the growth there is seen to be suppressed. However, the computation blows up at the time step about $n = 8500$ ($t \simeq 17$).

3. EVOLUTION EQUATIONS FOR THE PERTURBATION

For the leapfrog scheme

$$\mathbf{u}^{n+1} = \mathbf{u}^{n-1} + 2\Delta t \mathbf{F}(\mathbf{u}^n),$$

the solution can be expressed by the sum of the physical and computational modes: $\mathbf{u}^n = \mathbf{v}^n + (-1)^n \mathbf{w}^n$. The evolution equations for both modes are given by

$$\frac{d\mathbf{v}}{dt} = \frac{1}{2}[\mathbf{F}(\mathbf{v} - \mathbf{w}) + \mathbf{F}(\mathbf{v} + \mathbf{w})], \tag{10}$$

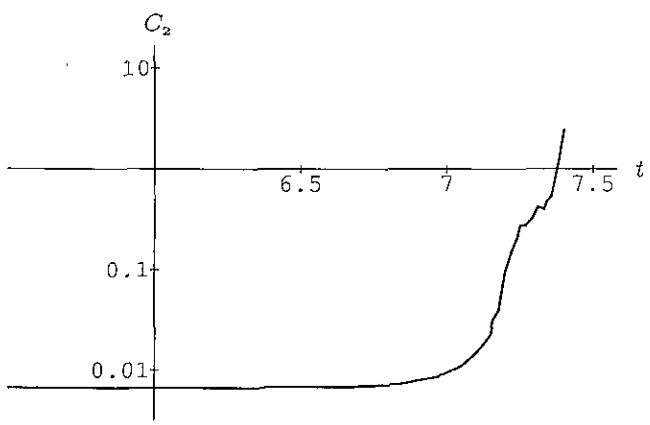

FIG. 2. Invariant C_2 for Figs. 1 as a function of time. C_2 is defined by Eq. (8). The computation blows up at $t \simeq 7.4$.

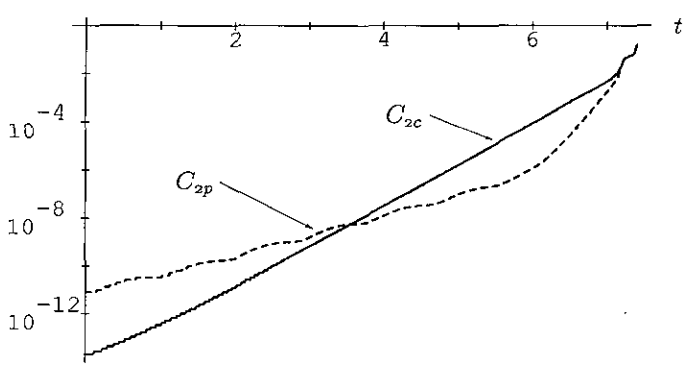

FIG. 3. C_{2p} and C_{2c} as functions of time corresponding to C_2 in Fig. 2.

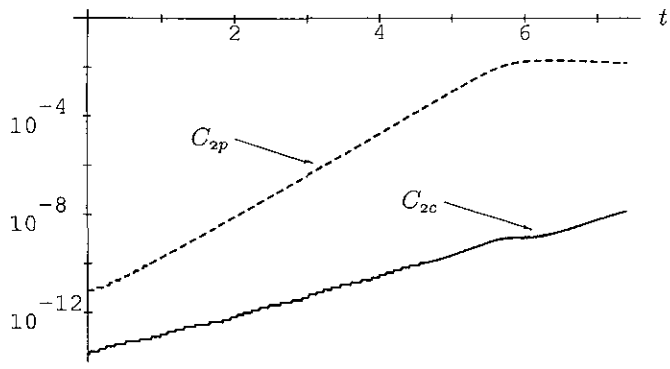

FIG. 4. C_{2p} and C_{2c} as functions of time for $\varepsilon = -0.1$. In this case the computation blows up at the time $t \simeq 17$.

$$\frac{d\mathbf{w}}{dt} = \frac{1}{2}[\mathbf{F}(\mathbf{v} - \mathbf{w}) - \mathbf{F}(\mathbf{v} + \mathbf{w})], \tag{11}$$

respectively [10]. In our case of the leapfrog scheme Eq. (6), the function $\mathbf{F}(\mathbf{u})$ can be written as

$$F_j(\mathbf{u}) = -\frac{1}{6\Delta x}(u_{j+1} + u_j + u_{j-1})(u_{j+1} - u_{j-1}).$$

When u_j^n is decomposed into v_j^n and w_j^n as expressed by Eq. (9), straightforward calculations of Eqs. (10) and (11) give

$$\frac{dv_j}{dt} = \frac{1}{6\Delta x}(v_{j+1} + v_j + v_{j-1})[2\varepsilon \cos\left(\frac{2\pi}{3}j\right) - (v_{j+1} - v_{j-1})] - \frac{1}{6\Delta x}(w_{j+1} + w_j + w_{j-1})(w_{j+1} - w_{j-1}), \tag{12}$$

$$\frac{dw_j}{dt} = -\frac{1}{6\Delta x}(w_{j+1} + w_j + w_{j-1})[2\varepsilon \cos\left(\frac{2\pi}{3}j\right) - (v_{j+1} - v_{j-1})] + \frac{1}{6\Delta x}(v_{j+1} + v_j + v_{j-1})(w_{j+1} - w_{j-1}). \tag{13}$$

At an earlier time stage $|v_j^n|$ and $|w_j^n|$ are considerably small compared to ε, so that Eqs. (12) and (13) are expressed approximately as

$$\frac{dv_j}{dt} = \frac{\varepsilon}{3\Delta x}(v_{j+1} + v_j + v_{j-1}) \cos\left(\frac{2\pi}{3}j\right), \tag{14}$$

$$\frac{dw_j}{dt} = -\frac{\varepsilon}{3\Delta x}(w_{j+1} + w_j + w_{j-1}) \cos\left(\frac{2\pi}{3}j\right), \tag{15}$$

Equations (14) and (15) indicate that for earlier times v_j^n and w_j^n evolve linearly independent of each other and that if the sign of ε is changed the temporal behavior of v_j^n and w_j^n is interchanged. The experimental evidence of the latter character is confirmed by Figs. 3 and 4.

Now let us consider the case where the solutions of Eqs. (14) and (15) become unstable. Equation (15) is different from (14) only in the sign of ε. Therefore the instability occurring in Eq. (15) can be predicted from the solution of Eq. (14) by changing the sign of ε. Focusing now on Eq. (14), it is obvious that it does not have the unstable one-mode solution of the form $v_j \propto e^{i2\pi j/3}$ considered by Briggs *et al.* [4], because for this mode it is always true that

$$v_{j+1} + v_j + v_{j-1} = 0.$$

Equation (14) contains one stationary mode of $e^{i2\pi j/3}$ in the cosine function which stems from the spatial derivative of the initial Fornberg's pattern. The three-mode solution composed of a superposition of the $e^{i2\pi j/3}$, $e^{i\pi j/3}$, and $e^{i\pi j}$ modes gives the simplest closed solution of Eq. (14) [4]. When a mode such as $e^{i(\pi/3+\delta)j}$ is stimulated, where $\delta = \pi\mu/J$ with μ being an integer [5], the modes which can be generated through interaction with the Fornberg mode $e^{i(2\pi/3)j}$ are only $e^{i(\pi/3-\delta)j}$ and $e^{i(\pi-\delta)j}$. Thus, in view of Eq. (9) we can write the solution of Eq. (14) in the form

$$v_j(t) = \xi(t)e^{i(\pi/3-\delta)j} + \eta(t)e^{i(\pi/3+\delta)j} + \zeta(t)e^{i(\pi-\delta)j} + \text{cc}, \tag{16}$$

where cc denotes complex conjugate terms. We note that the parameter δ is variable in the range of $0 \leq \delta \leq \pi/3$. As δ varies in this range, the amplitudes ξ, η, and ζ cover spectra in the range of $0 \sim \pi/3$, $\pi/3 \sim 2\pi/3$, and $2\pi/3 \sim \pi$, respectively. We also note that η and ζ represent the amplitudes of the sideband of the Fornberg's mode $e^{i2\pi j/3}$.

Substitution of Eq. (16) into Eq. (14) gives simultaneous differential equations for the amplitudes ξ, η, and ζ,

$$\frac{d\xi}{dt} = K_1\eta^* + K_3\zeta, \tag{17}$$

$$\frac{d\eta}{dt} = K_2\xi^* + K_3\zeta^*, \tag{18}$$

$$\frac{d\zeta}{dt} = K_2\xi + K_1\eta^*, \tag{19}$$

where

$$K_1 = \frac{\varepsilon}{6\Delta x}(1 + \cos\delta - \sqrt{3}\sin\delta),$$

$$K_2 = \frac{\varepsilon}{6\Delta x}(1 + \cos\delta + \sqrt{3}\sin\delta),$$

$$K_3 = \frac{\varepsilon}{6\Delta x}(1 - 2\cos\delta).$$

Equations (17)–(19) describe the temporal behavior of the amplitudes of the three modes which interact with each other through the stationary $e^{i2\pi j/3}$ mode. It should be noted that since the $e^{i2\pi j/3}$ mode is stationary the modes interact linearly. This

enables us to compose an arbitrary solution of v_j^n in Eq. (16) by superposing the solutions with different δ of ξ, η, and ζ in Eqs. (17)–(19).

4. UNSTABLE EXCITATION OF THE PERTURBATION

If we assume the solutions are of the form $e^{\lambda t}$ in Eqs. (17)–(19), λ can be obtained from the characteristic equation

$$[\lambda^3 + \alpha^3(\cos\delta)]^2 = 0, \tag{20}$$

where the function α of z is defined by

$$\alpha(z) \equiv \frac{\varepsilon}{3\Delta x}\left[\frac{1}{2}(2z-1)^2(z+1)\right]^{1/3}. \tag{21}$$

The three roots for λ are readily calculated from Eq. (20):

$$\lambda_1 = -\alpha, \quad \begin{pmatrix}\lambda_2\\ \lambda_3\end{pmatrix} = \frac{\alpha}{2} \pm i\frac{\sqrt{3}}{2}\alpha.$$

For the physical mode v_j^n, the sign of α is positive ($\varepsilon > 0$), so that the complex roots λ_2 and λ_3 give the unstable oscillatory solutions. The growth rate and the oscillation period are given by $\alpha/2$ and $4\pi/\sqrt{3}\alpha$, respectively; both depend on the sideband parameter δ. Maximum α is obtained from Eq. (21) as $\alpha_{\max} = \varepsilon/3\Delta x$ at $z = 1$ or $\delta = 0$. In our case of $\varepsilon = 0.1$ and $\Delta x = \frac{1}{120}$:

$$\frac{\alpha_{\max}}{2} = 2, \quad \frac{4\pi}{\sqrt{3}\alpha_{\max}} = 1.81,$$

while for the computational mode w_j^n, the sign of α is considered to be negative (corresponding to $\varepsilon < 0$), so that the only real root λ_1 gives the unstable solution. The maximum growth rate is $\alpha_{\max} = 4$. These results are in good agreement with the experimental results shown in Fig. 3.

One might be suspicious of setting $\delta = 0$, at which α takes its maximum value in Eq. (21). When $\delta = 0$ the independence between the amplitudes ξ and η disappears and ζ is no longer complex in Eq. (16). To examine the case of $\delta = 0$ we revise Eq. (16) as

$$v_j(t) = \xi(t)e^{i(\pi/3)j} + \xi^*(t)e^{-(i\pi/3)j} + \zeta(t)e^{ij},$$

where ζ is real. Then we obtain the amplitude equations

$$\frac{d\xi}{dt} = \frac{1}{2}\alpha(1)(2\xi^* - \zeta),$$

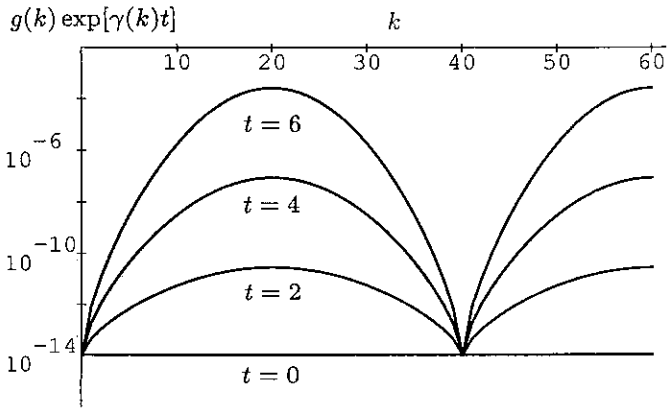

FIG. 5. Plots of $g(k)\exp[\gamma(k)t]$ for $t = 0$, 2, 4, and 6 as functions of the mode number k; $g(k) = 10^{-14}$; $\gamma(k)$ is the growth rate of the computational mode.

$$\frac{d\zeta}{dt} = \alpha(1)(\xi + \xi^*),$$

and the corresponding characteristic equation

$$\lambda^3 + \alpha^3(1) = 0.$$

Thus we find that Eq. (20) is valid for the case of $\delta = 0$.

If we denote the growth rate of the computational mode dependent upon the mode number k by $\gamma(k)$, the amplitudes of the excited spectrum will develop temporally as $\propto \exp[\gamma(k)t]$. For the physical mode they will develop as $\propto \exp[\frac{1}{2}\gamma(k)t]$. Figure 5 gives the plots of $g(k)\exp[\gamma(k)t]$ for $t = 0$, 2, 4, and 6, where the initial spectrum $g(k)$ is taken as $g(k) = 10^{-14}$, corresponding to the experimental results shown later. The growth rate $\gamma(k)$ has been calculated from $\alpha(z)$ in Eq. (21) for $\varepsilon = 0.1$ and $\Delta x = \frac{1}{120}$:

$$\gamma(k) = \alpha(\cos\delta), \quad \delta = \begin{cases} \pi(1/3 - k/J) & (0 \le k \le J/3), \\ \pi(k/J - 1/3) & (J/3 \le k \le 2J/3), \\ \pi(1 - k/J) & (2J/3 \le k \le J). \end{cases}$$

We obtained the Fourier mode spectra for both physical and computational modes experimentally from the discrete Fourier transform of v_j^n and w_j^n:

$$\begin{pmatrix}V_k^n\\ W_k^n\end{pmatrix} = \frac{1}{2J}\sum_{j=0}^{2J-1}\begin{pmatrix}v_j^n\\ w_j^n\end{pmatrix}\exp\left(-\frac{i\pi kj}{J}\right).$$

The resulting spectra $|W_k^n|$ at the time $t = 0$, 2, 4, and 6 are

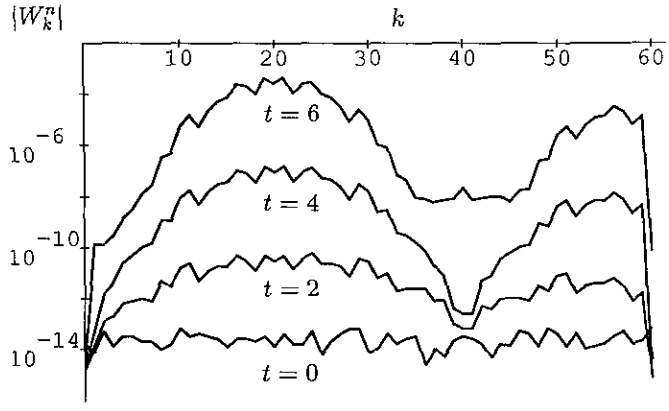

FIG. 6. Spectra of the computational mode $|W_k^n|$ corresponding to Fig. 5.

shown in Fig. 6, corresponding to the theoretical curves in Fig. 5. The figures correspond to C_{2c} in Fig. 3. The spectrum at $t = 0$ is the background noise ($\sim 10^{-14}$) generated when the missing starting values are calculated by the Runge–Kutta scheme. Comparison of these figures shows a good agreement of the gross excitation pattern in which the modes about $k = 20$ and 60 are predominant. Also, centering about them, there is growth which increases with time. A slight difference in the magnitude of the modes about $k = 60$ is observed. The mode at $k = 60$ is found not to be excited. The cause of these discrepancies is not well known, but it seems to be due to our linear analysis based on Eqs. (14) and (15).

Figure 7 shows the spectra $|V_k^n|$ corresponding to $|W_k^n|$ in Fig. 6. The dotted lines are plots of $g_1(k)\exp[\frac{1}{2}\gamma(k)t]$, where the initial spectrum is taken as $g_1(k) = 0.8 \times 10^{-11}$. The spectrum $|V_k^n|$ at $t = 0$ is composed of the spontaneous background noise plus the uniform random noise $\{r_j\}$ of order 10^{-11}. The sequence $\{r_j\}$ can be altered by changing the initial seed for the pseudorandom number generator. The spectra at $t = 2$ and 4 correspond

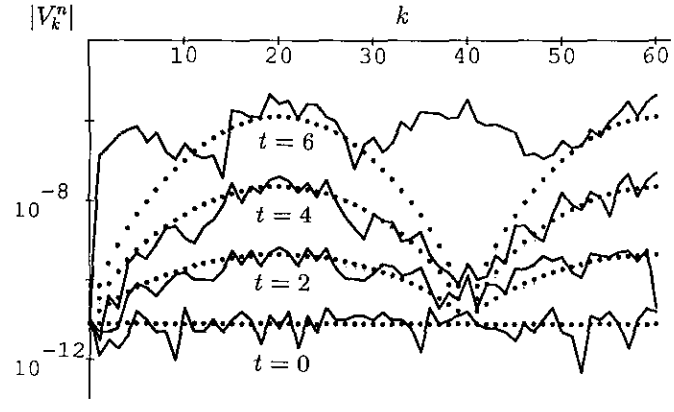

FIG. 7. Spectra of the physical mode $|V_k^n|$ corresponding to $|W_k^n|$ in Figs. 6. The dotted lines are plots of $g_1(k)\exp[\frac{1}{2}\gamma(k)t]$ for $t = 0$, 2, 4, and 6; $g_1(k) = 0.8 \times 10^{-11}$.

to the oscillatory change (with the growth rate of about $\gamma/2$) of C_{2p} in Fig. 3. In contrast to $|W_k^n|$, at the stage of $t = 6$ new modes about $k = 40$ and 5 are quickly excited, in addition to the old modes about $k = 20$ and 60. This stage corresponds to the exponential growth with the growth rate of about 2γ in C_{2p} shown in Fig. 3. These new modes are identified as the modes resulting from the product between the computational modes. This process is due to the last quadratic term of the computational modes on the right-hand side of Eq. (12). When the computational mode of the mode number k with the growth rate γ is multiplied by itself, it is converted to the physical mode of the mode number $2k$ with the growth rate 2γ. If $2k$ exceeds the maximum mode number J, the mode appears at $|2k - 2J|$ as aliasing errors. For confirmation of this process we eliminated the computational modes from the solution of Eq. (6) by applying the Runge–Kutta smoother [9] and we found that the new physical modes were not excited. Except for this purely nonlinear process the theoretical predictions for $|V_k^n|$ agree well with the experimental results. We found that the above-mentioned characteristics for $|W_k^n|$ and $|V_k^n|$ did not depend on the initial choice of the random sequence $\{r_j\}$ which was of order 10^{-11}.

5. CONCLUSIONS

In the present paper we have considered the unstable behavior of Fornberg's pattern under numerical integration using the leapfrog scheme Eq. (6). We have decomposed the solutions of Eq. (6) into the physical and computational modes and traced the temporal changes of the perturbation about Fornberg's pattern. To analyze the experimental results we derived the evolution equations for both physical and computational modes and discussed the unstable behavior of the perturbation about Fornberg's pattern. Thereby we have shown:

1. the perturbation about Fornberg's pattern is unstable for both physical and computational modes.
2. the instability occurs as the closed three-mode process and includes the side-band instability.

As we mentioned in the first section, the leapfrog instability can be suppressed by eliminating the computational mode if the instability is only due to the computational mode instability. The case studied in this paper shows that the physical mode can also be unstable, independent of the computational mode instability. In this case we cannot use the Runge–Kutta smoother to supppress the instability. To note this fact is important, although the case being considered may seem to be quite special. We are now examining the role of Fornberg's pattern contained in the spontaneous background noise.

ACKNOWLEDGMENTS

The author expresses his deep appreciation to M. Zimmer and R. Goldstein of the University of Illinois at Urbana-Champaign, for their careful reading of

the manuscript, and he is also grateful to Professor K. Abe, College of Arts and Sciences, the University of Tokyo, for continuous encouragement and support.

REFERENCES

1. B. Fornberg, *Math. Comput.* **27**, 45 (1973).
2. H. O. Kreiss and J. Oliger, *Tellus* **24**, 199 (1972).
3. F. Vadillo and J. M. Sanz-Serna, *J. Comput. Phys.* **66**, 225 (1986).
4. W. L. Briggs, A. C. Newell, and T. Sarie, *J. Comput. Phys.* **51**, 83 (1983).
5. D. M. Sloan and A. R. Mitchell, *J. Comput. Phys.* **67**, 372 (1986).
6. M. Mizutani, T. Niwa, and T. Ohno, *J. Math. Kyoto Univ.* **23**(1), 39 (1983).
7. J. M. Sanz-Serna, *SIAM J. Sci. Stat. Comput.* **6**, 923 (1985).
8. A. Aoyagi and K. Abe, *J. Comput. Phys.* **83**, 447 (1989).
9. A. Aoyagi and K. Abe, *J. Comput. Phys.* **93**, 287 (1991).
10. D. Cai, A. Aoyagi, and K. Abe, *J. Comput. Phys.* **107**, 146 (1993).